Proceedings of the Combustion Institute 40 (2024) 105243

Contents lists available at ScienceDirect

Proceedings of the Combustion Institute

journal homepage: www.elsevier.com/locate/proci

Uncertain lithium-ion cathode kinetic decomposition modeling via Bayesian chemical reaction neural networks

Benjamin C. Koenig [a], Huaibo Chen [a], Qiaofeng Li [a], Peng Zhao [b], Sili Deng [a,*]

[a] Department of Mechanical Engineering, Massachusetts Institute of Technology, Cambridge, MA 02139, USA
[b] Department of Mechanical, Aerospace, and Biomedical Engineering, University of Tennessee Knoxville, Knoxville, TN 37996, USA

ARTICLE INFO

Keywords:
Thermal runaway
Li-ion battery cathode decomposition
Uncertainty quantification
Chemical Reaction Neural Networks
Differential scanning calorimetry

ABSTRACT

Lithium-ion batteries are the focus of significant recent research interest due to their use in energy storage systems, electric vehicles, and other green technologies. Under various abuse conditions, these batteries undergo thermal runaway, which can lead to rapid temperature rise, flammable gas release, and fires. Current simulation approaches for thermal runaway at the full-cell scale involve utilizing kinetic models fit to experimental data from individual battery components. Despite substantial experimental uncertainty in the literature for these component experiments, prevalent models have not accounted for such uncertainty or noise. Here, we introduce uncertainty quantification for lithium-ion battery cathode thermal decomposition modeling via a novel Bayesian inference methodology. This approach leverages Chemical Reaction Neural Networks and particle-based uncertainty quantification to infer uncertain kinetic parameters while eliminating traditionally used simplifications, allowing for improvements to model accuracy and broader consideration of correlated parameters. We validated this new framework by learning an uncertain decomposition model for NCM333 (nickel-cobalt-manganese) cathode materials using differential scanning calorimetry (DSC) measurements with added synthetic noise. Then, we quantified the uncertainty in NCM811 cathode thermal runaway chemistry using experimental DSC measurements from various sources in the literature. Our methodology's ability to account for correlated Arrhenius parameters led to much broader uncertain parameter ranges and thus more generalizability at higher temperatures. We additionally found that the NCM811 model distribution learned directly from experimental data in the literature has 4σ onset temperature ranges up to 20 °C wide and specific reaction enthalpy ranges accounting for upwards of 80% of the mean value, carrying significant implications for downstream applications. Our work bridges the gap between noisy or uncertain experimental data and practical cell-scale simulations, thereby facilitating more realistic and robust thermal runaway models that support enhanced battery safety and performance optimization.

1. Introduction

Increasing demand for lithium-ion batteries in myriad applications including energy storage systems and electric vehicles has led to substantial recent research interest in the area. In addition to electrochemical performance, thermal runaway is a key aspect of novel technologies that must be considered in real-world applications. Abuse conditions such as overcharging, overheating, and penetration can lead to a cascade of exothermic reactions across battery components, internal short circuits, catastrophic temperature rise, and frequently combustible gas venting, fires, and explosions [1]. Developing accurate models to predict such catastrophic behavior is essential to mitigate safety concerns and will become more critical as batteries become more energy-dense and prolific.

Large-scale oven tests [2], accelerating rate calorimetry (ARC) [3,4], and fractional thermal runaway calorimetry (FTRC) [5] investigate the thermal runaway behavior of entire battery cells and can provide global modeling constraints and trends. To build models that describe this behavior, smaller-scale experiments like differential scanning calorimetry (DSC) [6–9] are needed to extract kinetic parameters and frameworks from component-level data. These kinetic models are used as the backbone for the more detailed, cell-scale simulations, from lumped thermal runaway in an ARC chamber [4,6] to multi-dimensional models [10] and even 3-D coupled multiphase combustion studies [11].

Traditionally, Kinetic models are extracted from DSC data via the Kissinger method [6,8,9,12,13], though this approach is limited in its assumption of reaction decoupling in multi-peak DSC data, which can

* Corresponding author.
E-mail address: silideng@mit.edu (S. Deng).

https://doi.org/10.1016/j.proci.2024.105243
Received 4 December 2023; Accepted 1 June 2024
Available online 24 June 2024

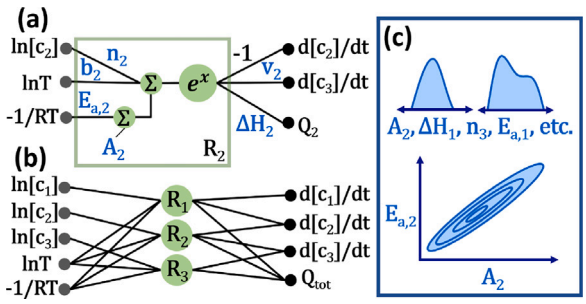

Fig. 1. Chemical reaction neural network, adapted from [15]. (a) A single neuron that exactly replicates Eq. (2) for R2. (b) Three stacked neurons to comprise the full reaction mechanism. The R_2 node contains the boxed green features in (a), with similar structures in R_1 and R_3. (c) Qualitative illustrations of individual and joint parameter distributions that are learned in this work.

lead to inaccurate kinetics [14,15]. To address this issue, the Chemical Reaction Neural Network (CRNN) approach [16,17] was recently generalized to learn thermal-kinetic models from battery component DSC data with multiple heat release peaks [15]. The CRNN structure eliminates the major assumptions made in the Kissinger approach, which enhances its accuracy to the data and to known decomposition processes. It also exactly satisfies the Arrhenius and mass action laws, allowing for its trained parameters to be directly used in larger-scale simulations.

However, a robust model must consider the inevitable uncertainties and variations in experimental data. Recent ARC experiments have shown strong cell-to-cell thermal runaway variation [4], largely induced by manufacturing inconsistency. Similar FTRC experiments also report substantial variability across functionally identical cells [5,18]. At the component scale, DSC experiments are typically conducted on disassembled cell components, introducing further uncertainties during disassembly and material processing [19] which lead to variability within and across data sources [6,15,19].

This uncertainty must be accounted for in kinetic models for reliable cell-scale thermal runaway simulations [19]. Recent work [4] performed uncertainty quantification on cell-scale ARC experiments, but focused on a simplified one-step global reaction model due to the sparse information contained in cell-level data. Other recent investigations studied the sensitivity of similar cell-scale simulations to uncertain thermophysical parameters, states of charge, and design configurations [20,21]. The crucial step of uncertainty quantification for component-scale kinetic models has been identified as essential for comprehensive and robust models that capture the intricate details of thermal runaway chemistry [19], but to our knowledge has not yet been studied.

The recently developed Bayesian CRNN (B-CRNN) methodology [22] integrates kinetic parameter uncertainty quantification into the CRNN framework and has been extended to studies with missing species, reversible reactions, enzymatic reactions, and biological systems [22,23], enabling the inference of uncertain component models that account for uncertain experimental data. In the original B-CRNN work, variational inference assuming independent parameters was used as an accelerated alternative to traditional Hamiltonian Monte Carlo (HCM). It becomes necessary, however, especially with temperature-dependent data and with all Arrhenius parameters calibrated (instead of only pre-exponential factors), to refine this assumption to adequately reflect the coupling between these parameters as governed by the Arrhenius rate law.

The major goal of this work is to develop uncertain models for component-scale kinetic reactions in lithium-ion batteries. To our knowledge, uncertainty quantification of thermal runaway kinetic models is a key issue that has not been addressed in the literature, and as the backbone of larger-scale, cell-level simulations such capability would have broad and meaningful applications. To do so, we propose a novel methodology that integrates Stein variational gradient descent [24] with the CRNN architecture in order to infer uncertain kinetic parameters for these models without the need for previously used simplifying assumptions. This novel inclusion of uncertainty will enable cell and pack-level simulations to provide mean values in addition to measures of the scientific community's confidence in the results, based on our knowledge of the component-level kinetics.

2. Methodology

To accurately quantify the uncertainty in battery thermal runaway chemistry from DSC data, we integrate Stein variational gradient descent (SVGD) into the CRNN architecture to account for the correlated parameter space. First, a single deterministic model is trained with the uncertain experimental data via CRNN (Section 2.1). This converged result then serves as the initialization for a distribution of models that capture the noisy data via SVGD (Section 2.2). Finally, Section 2.3 introduces the battery cathode DSC experiments to which we apply this novel methodology to demonstrate its capabilities.

2.1. Kinetic modeling via chemical reaction neural networks

In this study, we investigate the decomposition behavior of nickel-cobalt-manganese (NCM) cathode materials using a three-step sequential reaction model. Pristine layered NCM cathodes thermally decompose, in order, to the first spinel phase ($LiMn_2O_4$-type), the second spinel phase (Mn_3O_4-type), and finally the rock salt [25]. These are accounted for with the normalized masses c_i, with $i = 1:4$ respectively indicating these four phases. For $i = 1:3$, the sequential decomposition reactions R1, R2, and R3 can be written as

$$c_i \longrightarrow \nu_i c_{i+1} + \Delta H_i, \tag{1}$$

where ΔH_i is the specific reaction enthalpy for reaction i, and ν_i is the product stoichiometric coefficient. The reaction rates r_i can be expressed using the logarithmic form of the Arrhenius and mass action Laws,

$$r_i = \exp(n_i ln[c_i] + lnA_i + b_i lnT - E_{a,i}/RT), \tag{2}$$

where n_i is the apparent reaction order, A_i is the exponential pre-factor, b_i is the non-linear temperature dependence factor, and $E_{a,i}$ is the activation energy. Finally, the total specific heat release rate Q_{tot} is the sum of each reaction's contribution Q_i,

$$Q_{tot} = \sum_i Q_i = \sum_i \Delta H_i r_i. \tag{3}$$

As in [15], the model with three sequential reactions here is chosen (over simpler single peak or independent reaction models) based on its agreement with experimental DSC data and with fundamental phase change studies in the literature [25]. Here, we take Eq. (2) and insert it into the CRNN structure of Fig. 1. As per the standard CRNN methodology [15–17], we integrate the species gradient outputs to compute the network's predicted concentration and heat release profiles. The loss function is then defined as the mean absolute error between the experimental heat release data and the CRNN prediction,

$$Loss = \sum_j |Q_{tot,j} - Q_{tot,j}^{CRNN}|, \tag{4}$$

and the parameters are updated similarly to a neural ODE [26] via the gradient of this loss function, using the ADAM optimizer with a learning rate of 10^{-3}. Once this deterministic model converges, it is used to initialize the SVGD-based uncertain algorithm.

2.2. Uncertainty quantification via Stein variational gradient descent

To incorporate uncertainty, we couple this CRNN approach with SVGD [24] by defining a set of particles, each a distinct kinetic model, and then updating their parameters via a specialized form of gradient descent to form a model distribution that captures the uncertainty in a given dataset. This methodology removes the mean field approximation of the Bayes by Backprop (BBB) approach used in the B-CRNN algorithm of [22], while avoiding the high-cost pitfall of HMC sampling identified in [22]. To approximate the parameter distribution $p(\mathbf{x})$ that governs the uncertain data, we initialize m particles x_i $(i = 1, \dots, m)$ around the deterministic CRNN model. Each particle x is a vector of the 17 parameters A_i, b_i, $E_{a,i}$, n_i, ν_i, and ΔH_i that define the model of Eqs. (1)–(3), and the their converged distribution is trained to best capture $p(x)$. The gradient direction $\phi(\mathbf{x})$ is defined as

$$\phi(\mathbf{x}) = \frac{1}{m}\sum_{j-1}^{m}[\underbrace{k(\mathbf{x_j},\mathbf{x})\nabla_{\mathbf{x_j}}\log p(\mathbf{x_j})}_{\text{smoothed gradient}} + \underbrace{\nabla_{\mathbf{x_j}}k(\mathbf{x_j},\mathbf{x})}_{\text{repulsive}}], \tag{5}$$

which includes two terms. Qualitatively, the first term pushes the models $\mathbf{x}$ toward higher probability areas of $p(\mathbf{x})$ via a distance-smoothed gradient (similar to standard gradient descent), while the second term provides a repulsive force driving a given model $\mathbf{x}$ away from its close neighbors. In sum, these two terms aim to minimize the data reconstruction error of the m models while forcing them to differ from each other (according to noise and data functions defined below) substantially enough to effectively match $p(\mathbf{x})$ with the resulting distribution of model parameters.

In more mathematical detail, $k(\mathbf{x_j},\mathbf{x})$ is the radial basis function kernel defined identically as in [24],

$$k(\mathbf{x_j},\mathbf{x}) = exp(-\frac{1}{h}\|\mathbf{x_j}-\mathbf{x}\|^2), \tag{6}$$

where the bandwidth h is defined as

$$h = med(\mathbf{x})/\log(n), \tag{7}$$

with $med(\mathbf{x})$ as the median pairwise distance between the set of current points $\mathbf{x_i}$. The likelihood function is evaluated as

$$\log p(\mathbf{x}) = -\frac{1}{m}\sum_{k}\sum_{j}\left\|\frac{Q_j^{CRNN}(\mathbf{x}) - Q_{k,j}^{exp}}{w_j^{-1}\cdot\tau}\right\|_2^2, \tag{8}$$

where $\mathbf{Q}^{CRNN}(\mathbf{x})$ is the CRNN's heat release profile given the parameters $\mathbf{x}$, $\mathbf{Q}_k^{exp}$ is the kth dataset, j is the current index within a dataset, τ is a normalization factor defined for each reaction as the average standard deviation across all uncertain datasets at a given heating rate, and finally w_j is a user-defined weight (default $w_j = 1$) to facilitate extracting noise-masked peaks, as in [15]. Further discussion, theory, and analysis of this inference approach are available in [24]. Here, we emphasize that its particle-based nature inherently captures the correlation between kinetic parameters, which we find later in Section 3.1 to be of large importance for these decomposition models. The relatively expensive gradients of Eq. (8) can additionally be solved in parallel to maintain computational feasibility.

The DifferentialEquations [27] and ForwardDiff [28] packages in Julia are used for learning. The SVGD's converged parameter distributions are agnostic to the initialization [24], so we initialize the m particles simply as the deterministic model with 1% noise added. The particles are updated via gradient descent according to Eq. (5) with multithreaded $\nabla_{\mathbf{x}}\log p(\mathbf{x})$ calculations and a learning rate initialized as 2×10^{-4} and decaying 5% every 500 epochs.

2.3. Validation and target data

To validate the novel B-CRNN approach proposed here, we use the NCM333 decomposition data collected at five heating rates in [6]: 2, 5, 10, 15, and 20 °C/min. A deterministic model was previously trained for this data using a CRNN in [15] with generally strong performance but substantial inconsistencies across heating rates visible in certain regions of the data and model. Here we add 10% synthetic noise captured via 100 realizations (shown in Figs. 2 and S1) in addition to any experimental uncertainty already present in the data across heating rates, then demonstrate the capability of our novel B-CRNN approach in capturing both sources of uncertainty.

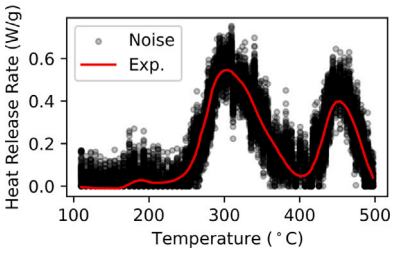

Fig. 2. Experimental DSC data for NCM333 decomposition from [6] at 20 °C/min (red curve), with 100 realizations of 10% synthetic noise added (black points). The full dataset used in Section 3.1 includes four additional heating rates shown in Fig. S1 (2, 5, 10, and 15 °C/min). (For interpretation of the references to color in this figure legend, the reader is referred to the web version of this article.)

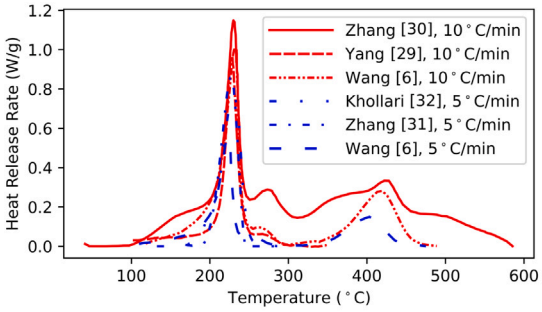

Fig. 3. Six experimental datasets for NCM811 decomposition used in Section 3.2, compiled from [6,29–32].

We then transition to uncertainty quantification assimilating experimental data collected by separate research groups. We choose the collection of NCM811 data obtained from [6,29–32] due to their similar charging, cleaning, and disassembly methodology, shown here in Fig. 3. In this demonstration, we move from mixed experimental and synthetic uncertainty toward pure experimental uncertainty to showcase the full capability of this B-CRNN approach and provide new insights to the community.

3. Results and discussion

3.1. Framework validation: NCM333 with synthetic noise

A single distribution of $m = 1000$ model parameters is learned that captures the noisy data at all heating rates shown in Figs. 2 and S1. Fig. 4 shows the results of this inference at the lowest and highest heating rates (all other heating rates are available in Figs. S2 and S3). Any discrepancies seen at a single heating rate are generally the result of systematic error across the heating rates. In [6,15], for example, where deterministic models were fit to the same (noise-free) data, the rightmost R3 peaks matched the 20 °C/min data at the cost of overpredicting the 2 °C/min data by up to a factor of two, effectively discarding this low heating rate information. Here, the B-CRNN instead predicts mean values that lie between the two datasets with a larger uncertainty range that captures this underlying systematic error in addition to the added synthetic noise, incorporating all of the information contained in the DSC data and allowing it to be passed forward to any cell-scale simulations built on these kinetic models.

A discrepancy is visible in the <200 °C range, where the SVGD 4-sigma result collapses to zero despite what appears to be a nonzero trend in the data. In practice, the SVGD has only three reactions available (as per the phase change results of [25]), and the MSE loss function steers the R1 peak toward the more significant heat release behavior in the 200 °C–275 °C rather than then flat noise in the lower temperature range. This nonzero behavior below 200 °C is not a true experimental trend and is instead an artifact of the synthetic noise-adding process (see the underlying data in Fig. 2). A fourth reaction R0 could be added to capture this remaining flat noise, though due to the artificial source of such noise and the phase change sequences and temperature ranges reported in the literature [6,15,25], we expect such a modification would be superficial and incorrect. Section 3.2 learns uncertain kinetic models from data without such artificial noise. In addition to uncertain model predictions, we provide Fig. 5a demonstrating the near-perfect correlation between the frequency factor and activation energies for the learned models. We recall Eq. (2) defining the exponential scaling of the reaction rate with $lnA_i - E_{a,i}/RT$. Given the narrow temperature windows for each reaction's heat release in the studied DSC data, it is unsurprising that the frequency factor and activation energy distribution of Fig. 5a form nearly a straight line with slope proportional to RT evaluated at a characteristic temperature for R1. We plot this exponential relationship in Fig. 5a at the characteristic R1 temperature $T_c = 275$ °C to emphasize this point, where the relatively small deviations orthogonal to this line result in the model prediction variation seen in Fig. 4.

To emphasize the significance of this correlation, we additionally inferred the kinetic parameters via the BBB-based algorithm proposed in [22,33], which does not account for such parameter correlation. The model predictions differ slightly as seen in Fig. 5b due to the different assumptions made in the BBB and SVGD algorithms, though both reconstruct the data reasonably. Fig. 5a shows a significant departure in overall parameter ranges, however, with the BBB models clustering without correlation around a single mean value. This result is unsurprising given the mean-field approximation of the BBB methodology, which was originally developed for black-box neural networks that do not need to account for physical law-enforced correlations such as that of Eq. (2). Here, however, it is evident that such an approximation leads to dramatically underreported uncertainty on the Arrhenius parameters.

While this appears to have only a moderate impact on the model predictions of Fig. 5b, we recall that DSC-based kinetic parameter inference is typically carried out with the intent to inform larger, cell-scale thermal runaway models with practical applications [4,6,10,11] where temperatures can approach and exceed 1000K. For such extrapolation, it is important to quantify the more complete range of correlated kinetic parameters reported by the SVGD-based algorithm used here, as the temperature-dependent behavior manifests substantially differently at elevated temperatures (based on Eq. (2)) and may not adhere to the truncated range of parameters reported by the BBB approach.

The kinetic parameters of the final 1000 SVGD models are available in the Supplementary Material.

3.2. Uncertainty quantification of NCM811 thermal decomposition kinetics

After validating and demonstrating the merits of the framework in capturing kinetic uncertainty with correlated parameters, we apply it to NCM811 DSC data. The DSC studies used [6,29–32] report similar experimental procedures, but have significant heat release variation across datasets. A direct numerical integral of the data in Fig. 3 from the initial temperature up to 275 °C, for example, reveals total heat release amounts in a wide range from 154 J/g to 293 J/g. We additionally observe in the data from [30] a substantial amount of background heat release in the higher temperature regions, which may be an accurate measurement or an experimental drift that requires baseline shifting to correct. Additionally notable from inspection of Fig. 3 is a large variation at around 200 °C in heat release onset temperatures, which

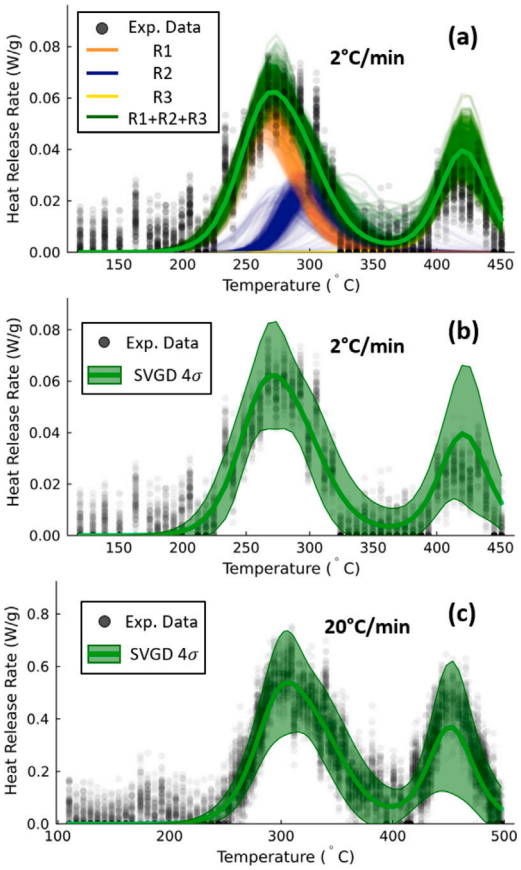

Fig. 4. Framework validation predictions for NCM333 data with 10% synthetic noise. Noisy experimental data shown as gray circles in all plots. (a) SVGD model predictions for R1, R2, R3, and their sum at 2 °C/min. (b), (c) 4σ uncertainty ranges predicted by the SVGD model at 2 °C/min and 20 °C/min, respectively. Good agreement is seen not only within each noisy dataset but also across the systematic error between datasets. All results predicted by this model (2, 5, 10, 15, and 20 °C/min) are available in Figs. S2 and S3.

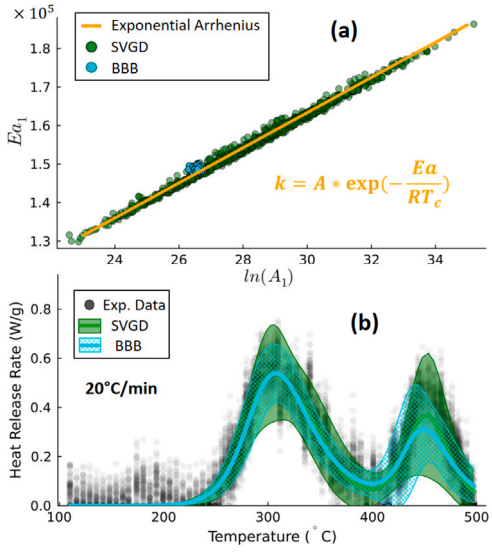

Fig. 5. (a) Correlations between the activation energy and frequency factor for R1 considering all heating rates. The exponential Arrhenius relation between these two values is plotted at $T_c = 275$°C, a characteristic temperature for R1 across all heating rates, to illustrate the origin of the strong correlation seen here. (b) 4σ uncertain model predictions shown at just 20 °C/min for brevity. Despite similar DSC predictions, the BBB method reports a severely limited parameter range due to the lack of consideration of coupling via the Arrhenius law.

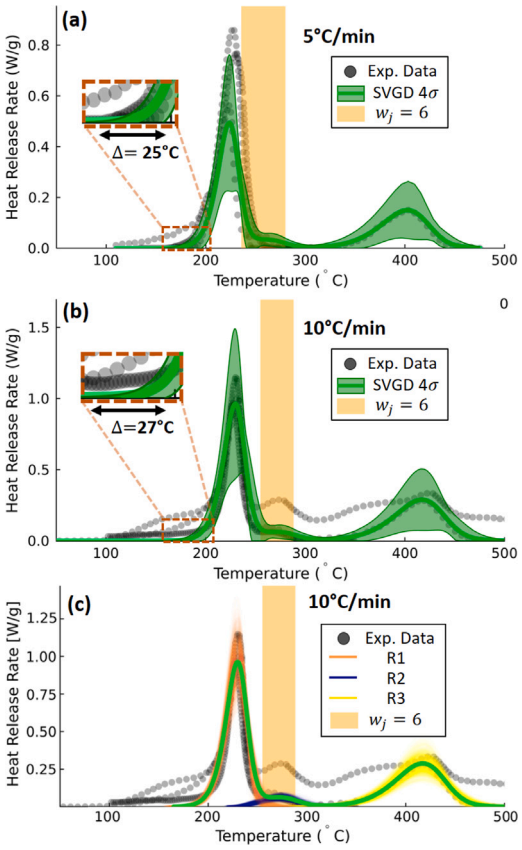

Fig. 6. NCM811 uncertainty quantification results at (a) 5 °C/min and (b, c) 10 °C/min. (a) and (b) show 4σ uncertainty ranges, while (c) shows R1, R2, and R3 realizations (R1+R2+R3 realizations are omitted for clarity, as the peaks do not overlap substantially like in Fig. 4). Experimental data shown as gray circles in all plots. Notable discrepancy in R3 reconstruction likely stems from sparse data in general and specifically in the >350 °C range, otherwise, R1 and R2 appear to follow the data and its variations well. Uncertain heat release onset temperature ranges are shown in zoomed views in (a) and (b) (also tabulated in Table 1). These large ranges imply significant uncertainty in cathode exothermic behavior onset in the practical, cell-scale simulations that the current kinetic models are developed for.

along with uncertainty in the total amount of heat released is a key metric for thermal runaway potential. In summary, the NCM811 data compiled from the literature shows substantial and inconsistent uncertainty across its three heat release peaks, and the use of deterministic parameters to describe this data could lead to large errors in practical, cell-scale simulations.

Since some experiments shown in Fig. 3 observe the R2 peak, when we apply the proposed B-CRNN framework to this dataset, the weight in Eq. (8) is changed to $w_j = 6$ in the shaded regions to ensure the reconstruction of its small and noise-masked peak. We use $m = 500$ particles to learn a single distribution of kinetic parameters across all six of these datasets. The uncertain prediction ranges predicted by the learned model distribution are shown in Fig. 6. The overall 4σ prediction ranges follow what is seen in the data fairly well. The range of peak heat release rates for R1 is very wide, as expected from the substantial uncertainty in the experimental data.

Reaction R3 is not as essential to cell-scale thermal runaway due to its smaller overall heat release and its late initiation. By 400 °C, it is likely that an internal short circuit and catastrophic heat release have already occurred. As a possible result of this, only three of the cited studies collected data up to and through the heat release of R3. Due to the reduced amount of data as well as the previously discussed background noise, the SVGD prediction for this peak has what appears to be a larger-than-needed uncertainty range. A prior distribution from a previously learned uncertain model could shrink this uncertain range and steer the current model toward prior knowledge, though such a prior is not available in the literature. If a clearer understanding of the R3 chemistry is desired, repeated experiments or additional datasets from other sources can be added to the inference process.

Table 1
Key metrics of uncertain NCM811 kinetic models.

Measure	Mean	Std.	4σ range
T_{on}, 5 °C/min	199.2	2.4	19.2
T_{on}, 10 °C/min	204.8	2.0	16
ΔH_1 (J/g)	165	17.3	138.4
ΔH_2[a] (J/g)	35.4	4.1	32.8
ΔH_3[a] (J/g)	177.1	19.0	152
lnk_1, 225 °C	−4.55	0.07	0.58
lnk_2, 275 °C	−4.31	0.24	1.92
lnk_3, 410 °C	−5.16	0.13	1.04

[a] Per gram of reactant c_i (see Eq. (1)).

Statistics of the inferred uncertain models for NCM811 thermal decomposition chemistry are reported in Table 1. Taking the tangent line of a DSC prediction defined at the point of the largest slope, we define the onset temperature traditionally as its intersection with the temperature axis. The reaction rate constants are defined as $k_i = A_i T^{b_i} exp(-Ea_i/RT)$, with characteristic temperatures chosen for each reaction based on their peak heat release rate location in Fig. 6. Following the observation of the experimental data, the 4σ uncertain ranges on the reaction enthalpies are substantial and nearly span the entire mean value. The standard deviation itself in all three of these measures is already greater than 10% of the mean value. The onset temperature ranges, which depend strongly on the Arrhenius parameters of k_i, additionally contain large uncertainty (see Fig. 6 insets for a visualization of this quantity and its 4σ range). This uncertainty will propagate forward to cell-level simulations, where it indicates significant variation in the heat release window leading directly to internal short circuit [6]. The transition from deterministic to uncertain kinetic parameters lets modelers capture much more of the interesting variation seen at the DSC component scale and creates more meaningful and realistic models that can better inform cell-scale thermal runaway simulations.

The kinetic parameters of the final 500 SVGD models are available in the Supplementary Material.

3.3. Discussion of practical applications for uncertain models

DSC-based investigations usually focus solely on new data, not leveraging existing literature. Instead, we propose a framework that combines data from the literature to learn uncertain parameters for thermal runaway UQ, aligning with the chemical kinetics field's iterative model improvement process using diverse datasets. Bayesian inference, being a continual learning framework, allows future efforts to build on previous posterior distributions, incorporating new results into the existing literature.

Quantifying uncertainty in component-level thermal runaway kinetics informs cell-scale thermal runaway simulations. In computationally inexpensive 0-D ARC simulations, the uncertain models learned by this B-CRNN tool can be directly propagated forward for thermal runaway predictions. Scaling up to 2-D or 3-D conduction models or complex multiphase models with heat generation, conduction, pressure buildup/release, and gas-phase combustion makes direct propagation of hundreds of kinetic models impractical. Efficient uncertainty quantification techniques from the chemical kinetics literature, such as response surfaces [34,35], neural network-based surrogates [36–38], and dimension reduction tools [39–41], may aid in sampling SVGD-inferred models for computationally intensive multidimensional thermal runaway simulations.

4. Conclusions

This study focused on quantifying the kinetic uncertainty of battery cathode thermal runaway kinetics and investigating the correlation among the uncertain model parameters. We accomplished this by developing a methodology for inferring uncertain kinetic parameters from DSC data using CRNNs trained via SVGD. This technique leverages CRNN's ability to learn multi-step kinetics from DSC profiles while providing uncertain parameters with correlated distributions that capture more general and temperature-dependent effects that prior CRNN-based UQ methods have missed. We validated this methodology using a case with added noise and demonstrated its robustness and practicality in real-world scenarios by applying it to experimental data taken from diverse sources in the literature. We successfully quantified substantial experimental uncertainty in this data and reported various statistical characteristics of the resultant models.

When scaling up to practical, large-scale thermal runaway simulations, the kinetically interpretable framework of the CRNN allows for these uncertain kinetic models to be directly applied in cell-scale simulations. Given the ongoing challenges in the literature surrounding reliable model development for catastrophic thermal runaway prediction, the sensitivity of various thermal runaway metrics to component-level kinetics, and the dearth of uncertainty quantification methodologies or considerations for such reactions, this introduction of component-scale kinetic uncertainty will provide useful insights and constraints for downstream modeling applications.

Novelty and significance statement

This research introduces uncertainty quantification (UQ) for lithium-ion battery thermal runaway kinetic modelling by proposing a novel and generalized Bayesian inference methodology. It is motivated by substantial discrepancies observed in the literature between experimental data collected by different research groups, and to the authors' knowledge has not previously been considered in the literature from a modelling perspective. Tackling this problem is significant due to the increasing reliance of electric vehicles and energy storage systems on batteries with higher energy densities and advanced materials that are more prone to catastrophic thermal runaway events, which these uncertain models can help to provide practical engineering constraints for.

CRediT authorship contribution statement

Benjamin C. Koenig: Conceptualization, Methodology, Investigation, Writing. **Huaibo Chen:** Methodology. **Qiaofeng Li:** Methodology. **Peng Zhao:** Conceptualization, Editing. **Sili Deng:** Conceptualization, Editing, Project administration.

Declaration of competing interest

The authors declare that they have no known competing financial interests or personal relationships that could have appeared to influence the work reported in this paper.

Acknowledgments

The work is supported by the National Science Foundation (NSF) under Grant No. CBET-2143625. BCK is partially supported by the NSF Graduate Research Fellowship under Grant No. 1745302.

Appendix A. Supplementary data

Supplementary material for this article is provided.

Supplementary material related to this article can be found online at https://doi.org/10.1016/j.proci.2024.105243.

References

[1] Q. Wang, B. Mao, S.I. Stoliarov, J. Sun, A review of lithium ion battery failure mechanisms and fire prevention strategies, Prog. Energy Combust. Sci. 73 (2019) 95–131.

[2] T.D. Hatchard, D.D. MacNeil, A. Basu, J.R. Dahn, Thermal model of cylindrical and prismatic lithium-ion cells, J. Electrochem. Soc. 148 (7) (2001) A755.

[3] B. Lei, W. Zhao, C. Ziebert, N. Uhlmann, M. Rohde, H.J. Seifert, Experimental analysis of thermal runaway in 18650 cylindrical Li-ion cells using an accelerating rate calorimeter, Batteries 3 (2) (2017) 14.

[4] L. Zhang, S. Yang, L. Liu, P. Zhao, Cell-to-cell variability in Li-ion battery thermal runaway: Experimental testing, statistical analysis, and kinetic modeling, J. Energy Storage 56 (2022) 106024.

[5] W.Q. Walker, K. Cooper, P. Hughes, I. Doemling, M. Akhnoukh, S. Taylor, J. Darst, J. Billman, M. Sharp, D. Petrushenko, R. Owen, M. Pham, T. Heenan, A. Rack, O. Magdsyuk, T. Connolley, D. Brett, P. Shearing, D. Finegan, E. Darcy, The effect of cell geometry and trigger method on the risks associated with thermal runaway of lithium-ion batteries, J. Power Sources 524 (2022) 230645.

[6] Y. Wang, D. Ren, X. Feng, L. Wang, M. Ouyang, Thermal kinetics comparison of delithiated $Li[Ni_xCo_yMn_{1-x-y}]O_2$ cathodes, J. Power Sources 514 (2021) 230582.

[7] D. Ren, X. Liu, X. Feng, L. Lu, M. Ouyang, J. Li, X. He, Model-based thermal runaway prediction of lithium-ion batteries from kinetics analysis of cell components, Appl. Energy 228 (2018) 633–644.

[8] D.D. MacNeil, J.R. Dahn, The reactions of $Li_{0.5}CoO_2$ with nonaqueous solvents at elevated temperatures, J. Electrochem. Soc. 149 (7) (2002) A912.

[9] A. Kriston, I. Adanouj, V. Ruiz, A. Pfrang, Quantification and simulation of thermal decomposition reactions of Li-ion battery materials by simultaneous thermal analysis coupled with gas analysis, J. Power Sources 435 (2019) 226774.

[10] H. Chen, J.E.H. Buston, J. Gill, D. Howard, R.C.E. Williams, E. Read, A. Abaza, B. Cooper, J.X. Wen, A simplified mathematical model for heating-induced thermal runaway of lithium-ion batteries, J. Electrochem. Soc. 168 (1) (2021) 010502.

[11] P. Zhang, J. Lu, K. Yang, H. Chen, Y. Huang, A 3D simulation model of thermal runaway in Li-ion batteries coupled particles ejection and jet flow, J. Power Sources 580 (2023) 233357.

[12] H.E. Kissinger, Variation of peak temperature with heating rate in differential thermal analysis, J. Res. Natl. Bur. Stand. 57 (4) (1956) 217.

[13] H. Wang, A. Tang, K. Huang, Oxygen evolution in overcharged $Li_xNi_{1/3}Co_{1/3}Mn_{1/3}O_2$ electrode and its thermal analysis kinetics, Chin. J. Chem. 29 (8) (2011) 1583–1588.

[14] S. Vyazovkin, Kissinger method in kinetics of materials: Things to beware and be aware of, Molecules (Basel, Switzerland) 25 (12) (2020) E2813.

[15] B.C. Koenig, P. Zhao, S. Deng, Accommodating physical reaction schemes in DSC cathode thermal stability analysis using chemical reaction neural networks, J. Power Sources 581 (2023) 233443.

[16] W. Ji, S. Deng, Autonomous discovery of unknown reaction pathways from data by chemical reaction neural network, J. Phys. Chem. A 125 (4) (2021) 1082–1092.

[17] W. Ji, F. Richter, M.J. Gollner, S. Deng, Autonomous kinetic modeling of biomass pyrolysis using chemical reaction neural networks, Combust. Flame 240 (2022) 111992.

[18] W.Q. Walker, J.J. Darst, D.P. Finegan, G.A. Bayles, K.L. Johnson, E.C. Darcy, S.L. Rickman, Decoupling of heat generated from ejected and non-ejected contents of 18650-format lithium-ion cells using statistical methods, J. Power Sources 415 (2019) 207–218.

[19] C. Lenz, J. Hennig, W. Tegethoff, H.-G. Schweiger, J. Koehler, Analysis of the interaction and variability of thermal decomposition reactions of a Li-ion battery cell, J. Electrochem. Soc. 170 (6) (2023) 060523.

[20] A.S. Yeardley, P.J. Bugryniec, R.A. Milton, S.F. Brown, A study of the thermal runaway of lithium-ion batteries: A Gaussian process based global sensitivity analysis, J. Power Sources 456 (2020) 228001.

[21] W. Zhang, J. Yuan, J. Huang, Y. Xie, Uncertainty assessment method for thermal runaway propagation of lithium-ion battery pack, Appl. Therm. Eng. (2023) 121946.

[22] Q. Li, H. Chen, B.C. Koenig, S. Deng, Bayesian chemical reaction neural network for autonomous kinetic uncertainty quantification, Phys. Chem. Chem. Phys. 25 (5) (2023) 3707–3717.

[23] E. Nieves, R. Dandekar, C. Rackauckas, Uncertainty quantified discovery of chemical reaction systems via Bayesian scientific machine learning, Front. Syst. Biol. 4 (2024).

[24] Q. Liu, D. Wang, Stein variational gradient descent: A general purpose Bayesian inference algorithm, in: Advances in Neural Information Processing Systems, Vol. 29, 2016.

[25] S.-M. Bak, E. Hu, Y. Zhou, X. Yu, S.D. Senanayake, S.-J. Cho, K.-B. Kim, K.Y. Chung, X.-Q. Yang, K.-W. Nam, Structural changes and thermal stability of charged $LiNi_xMn_yCo_zO_2$ cathode materials studied by combined *in situ* time-resolved XRD and mass spectroscopy, ACS Appl. Mater. Interfaces 6 (24) (2014) 22594–22601.

[26] R.T.Q. Chen, Y. Rubanova, J. Bettencourt, D. Duvenaud, Neural ordinary differential equations, 2019, arXiv:1806.07366 [cs, stat].

[27] C. Rackauckas, Q. Nie, DifferentialEquations.jl – A performant and feature-rich ecosystem for solving differential equations in julia, J. Open Res. Softw. 5 (1) (2017) 15.
[28] J. Revels, M. Lubin, T. Papamarkou, Forward-mode automatic differentiation in julia. arXiv:1607.07892 [cs].
[29] L. Yang, J. Zhang, W. Xue, J. Li, R. Chen, H. Pan, X. Yu, Y. Liu, H. Li, L. Chen, X. Huang, Anomalous thermal decomposition behavior of polycrystalline $LiNi_{0.8}Mn_{0.1}Co_{0.1}O_2$ in PEO-based solid polymer electrolyte, Adv. Funct. Mater. 32 (23) (2022) 2200096.
[30] F. Zhang, C. Wu, K. Li, T. Deng, A comparative analysis on thermal stability of delithiated nickel-rich $LiNi_{0.8}Co_{0.15}Al_{0.05}O_2$ and $LiNi_{0.8}Co_{0.1}Mn_{0.1}O_2$ in Pouch Cells, J. Electrochem. Energy Convers. Storage 21 (011006) (2023).
[31] M. Zhang, H. Zhao, M. Tan, J. Liu, Y. Hu, S. Liu, X. Shu, H. Li, Q. Ran, J. Cai, X. Liu, Yttrium modified Ni-rich $LiNi_{0.8}Co_{0.1}Mn_{0.1}O_2$ with enhanced electrochemical performance as high energy density cathode material at 4.5 V high voltage, J. Alloys Compd. 774 (2019) 82–92.
[32] M.A. Razmjoo Khollari, M.K. Azar, M. Esmaeili, N. Malekpour, S.M. Hosseini-Hosseinabad, R.S. Moakhar, A. Dolati, S. Ramakrishna, Electrochemical performance and elevated temperature properties of the TiO_2-coated $Li[Ni_{0.8}Co_{0.1}Mn_{0.1}]O_2$ cathode material for high-safety Li-ion batteries, ACS Appl. Energy Mater. 4 (5) (2021) 5304–5315.
[33] C. Blundell, J. Cornebise, K. Kavukcuoglu, D. Wierstra, Weight uncertainty in neural networks, 2015, arXiv:1505.05424 [cs, stat].
[34] H. Wang, D.A. Sheen, Combustion kinetic model uncertainty quantification, propagation and minimization, Prog. Energy Combust. Sci. 47 (2015) 1–31.
[35] B. Yang, Towards predictive combustion kinetic models: Progress in model analysis and informative experiments, Proc. Combust. Inst. 38 (1) (2021) 199–222.
[36] Y. Zhang, W. Dong, L.A. Vandewalle, R. Xu, G.P. Smith, H. Wang, Neural network approach to response surface development for reaction model optimization and uncertainty minimization, Combust. Flame 251 (2023) 112679.
[37] S. Li, B. Yang, F. Qi, Accelerate global sensitivity analysis using artificial neural network algorithm: Case studies for combustion kinetic model, Combust. Flame 168 (2016) 53–64.
[38] H. Chen, W. Ji, S.J. Cassady, A.M. Ferris, R.K. Hanson, S. Deng, Using shock tube species time-histories in Bayesian parameter estimation: Effective independent-data number and target selection, Proc. Combust. Inst. 39 (4) (2023) 5299–5308.
[39] W. Ji, J. Wang, O. Zahm, Y. Marzouk, B. Yang, Z. Ren, C. Law, Shared low-dimensional subspaces for propagating kinetic uncertainty to multiple outputs, Combust. Flame 190 (2018) 146–157.
[40] B.C. Koenig, W. Ji, S. Deng, Kinetic subspace investigation using neural network for uncertainty quantification in nonpremixed flamelets, Proc. Combust. Inst. (2022).
[41] B.C. Koenig, S. Deng, Multi-target active subspaces generated using a neural network for computationally efficient turbulent combustion kinetic uncertainty quantification in the flamelet regime, Combust. Flame 258 (2023) 113015.